The Influence of Coal Particle and Air Jet Momenta on MILD Combustion in a Recuperative Furnace

Emmet M. Cleary,[1,2] Paul R. Medwell[1*], Bassam B. Dally[1]
[1]School of Mechanical Engineering,
The University of Adelaide SA 5005, Australia;
[2]Department of Mechanical and Aerospace Engineering,
Princeton University NJ 08544, USA

Abstract

The moderate or intense low-oxygen dilution (MILD) combustion regime is a promising technology that operates at high combustion efficiency and lessens pollutant emissions. This numerical study of a parallel jet recuperative MILD combustion furnace investigates the effects of coal particle size and inlet air momentum on furnace dynamics and global CO emissions. It is found that coal particle size affects the coal penetration depth within the furnace and the location of a particle stagnation point. The effects of air inlet momentum are tested in two ways, first by raising the inlet temperature at constant mass flow rate, and second by increasing the mass flow rate at constant temperature. In both cases, increasing the air jet momentum broadens the reaction zone and facilitates MILD combustion, but also increases CO emissions due to lowered reaction rates.

Keywords: MILD combustion, coal combustion, jet momentum, CO

1. Introduction

Moderate or intense low-oxygen dilution (MILD) combustion is known to reduce pollutant emissions while improving energy efficiency. This combustion technique has been the subject of many studies, and is reviewed by Cavaliere *et al.* [1] and Li *et al.* [2] As coal is one of the most common and prevalent fossil fuels, studies on its application to MILD combustion technology are imperative. Still, MILD combustion of coal has received little attention among the industry and research communities.

A number of experimental studies have been conducted on the Adelaide MILD combustion furnace. One study focuses on NO_x scaling in the MILD combustion of natural gas, finding neither chemical nor mixing timescales controlled NO_x formation [3]. Later research with this furnace shifts towards stability studies and reports a critical ratio between air and fuel jet momentum that separates conventional and MILD combustion [4]. Other works with this furnace include experiments and simulations of premixed MILD combustion [5], oxy-fuel combustion [6], and biomass combustion [7]. In all cases where MILD combustion is successfully achieved, the authors report low NO_x and CO emissions, uniform and low combustion temperatures, and no visible flame.

Other research groups have performed experiments and simulations of MILD coal combustion. Stadler *et al.* [8] show experimentally and numerically that MILD combustion of coal yields lower NO_x emissions than conventional burners. Vascallari *et al*. [9] numerically test several turbulence-chemistry interaction models and report that the finite rate Eddy Dissipation Concept gives the best predictions to their experimental results.

This paper, while computational in nature, serves as a precursor for experimental work on MILD coal combustion in the Adelaide MILD combustion furnace. First, the furnace geometry, meshing, and all numerical models used are discussed. Then, results from 7 cases of simulations with different air inlet momenta and fuel particle momenta are presented and discussed.

2. Mild Combustion Simulations

2.1 Furnace Geometry and Mesh

The furnace modeled in this paper is the Adelaide MILD combustion furnace [3-4]. This recuperative furnace includes a central fuel jet (7.5 mm diameter) parallel to four air jets (4 mm diameter) and four exhausts (26.4 mm diameter), and two heat exchangers.

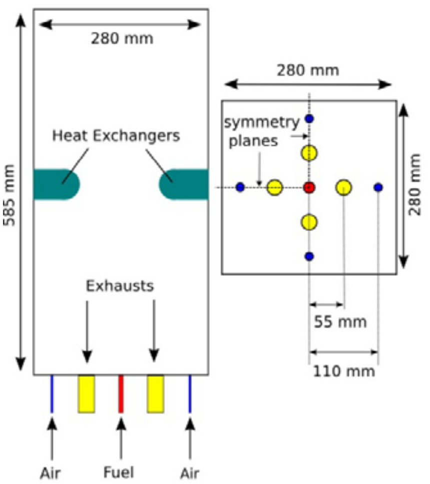

Figure 1: Side view (left) and top view (right) of the furnace modeled.

* Corresponding author:
Phone: (+61) 8 8313 5920
Email: paul.medwell@adelaide.edu.au

This study uses a 3D, structured, hexahedral mesh of 1.1 million cells, and models one quarter of the furnace geometry (Fig. 1). This simplification reduces computational expense but requires an assumption of a constant surface temperature of the heat exchanger. This approximation has little effect on furnace kinetics.

2.2 Numerical Models

All simulations presented in this work solve the steady Reynolds Averaged Navier Stokes (RANS) equations in the ANSYS Fluent v. 14.5 code. For consistency with previous numerical studies on this furnace, RANS equation closure uses the 2-equation realisable k-ε turbulence model [10] with the SIMPLE algorithm for pressure-velocity coupling. Coal particles are treated as a discrete phase and are tracked using a deterministic Lagrangian approach [11] to update particle source terms. Radiation modeling uses the discrete ordinates model [12]. All spatial discretisations follow the first order upwind scheme. Simulations are run using the Tizard supercomputer at eResearch SA on 24 cores, which took 720 hours for the base case and approximately 340 hours for each subsequent case.

2.3 Chemical Mechanisms and Models

The combustion model uses finite rate chemistry with the Eddy Dissipation Concept model [13] for chemistry-turbulence interaction. The multiple surface reactions combustion model is used for a 6-reaction chemical mechanism, which includes volatile combustion and char burnout:

$$C_xH_yO_zN_lS_n + \left(\frac{x}{2}+\frac{y}{2}-\frac{z}{2}+n\right)O_2 \rightarrow xCO + \frac{y}{2}H_2O + \frac{l}{2}N_2 + nSO_2 \quad (1)$$

$$CO + \frac{1}{2}O_2 \rightarrow CO_2 \quad (2)$$

$$C_{char} + \frac{1}{2}O_2 \rightarrow CO \quad (3)$$

$$C_{char} + CO_2 \rightarrow 2CO \quad (4)$$

$$C_{char} + H_2O \rightarrow H_2 + CO \quad (5)$$

$$H_2 + \frac{1}{2}O_2 \rightarrow H_2O \quad (6)$$

Variables *x*, *y*, *z*, *l*, and *n* are found from the ultimate analysis of the coal used (refer section 2.4). Refer to Table 1 for the Arrhenius coefficients.

2.4 Coal Characteristics

Coal characteristics follow proximate and ultimate analyses of Kingston brown coal (Table 2) with a calorific value of 20.0 MJ/kg. Particle sizes range from 38 to 180 μm in diameter and follow a Rosin-Rammler distribution. Coal devolatilisation follows a single-rate model according to Kobayashi et al. [19], using Arrhenius coefficients of A = 6.6×10^4 s^{-1} and E_a = 1.06×10^5 J/kgmol.

Table 1: Arrhenius coefficients for reactions (1-6).

Reaction	A	E_a (J/kgmol)	Reference
(1)	4.84×10^7	5.1×10^7	[14]
(2)	1.3×10^{11}	1.26×10^8	[15]
(3)	0.005	7.4×10^7	[16]
(4)	0.00635	1.62×10^8	[17]
(5)	0.00192	1.47×10^8	[17]
(6)	9.87×10^8	3.1×10^7	[18]

Table 2: Proximate and ultimate analyses (%db) of coal used.

Proximate analysis		Ultimate analysis	
Ash	21.6	C	52.5
Volatiles	42.7	H	3.60
Fixed Carbon	35.7	O	17.73
		N	0.48
		S	4.09

Table 3: Summary of cases.

Case	Particle diameter (μm)	Air temperature (K)	Air mass flow rate (g/s)
1	38-180	300	1.27
2	38	300	1.27
3	180	300	1.27
4	38-180	400	1.27
5	38-180	500	1.27
6	38-180	300	1.48
7	38-180	300	1.77

2.5 Simulation Parameters and Cases

For all simulations in this paper, the fuel stream has a mass flow rate of 0.236 g/s of coal in a carrier gas of CO_2 at 7.79 m/s and 300 K. The cases of interest are summarised in Table 3. First, the influence of particle diameter is presented at a constant inlet fuel and air jet momentum ratio (cases 1-3). Second, the inlet air jet momentum is increased at constant mass flow rate through air preheating (cases 1, 4 and 5). Lastly, the inlet air jet momentum is increased at constant temperature by increasing the mass flow rate (case 1, 6 and 7). In all cases, fuel inlet temperature is kept at 300 K, and the wall and heat exchanger temperatures are held at constant values of 1150 K and 450 K respectively.

3. Results and Discussion

3.1 Effects of Coal Particle Diameter

Comparison of the velocity fields for cases 1-3 show that the coal particle diameter has only a slight effect on furnace performance (results not shown for brevity). However, the particle tracks for these cases differ noticeably due to the higher Stokes numbers of larger (heavier) particles. In all cases, the momentum of the air jet dominates that of the fuel jet, creating a stagnation point some distance above the fuel jet, as shown pictorially in Fig. 2. The height of the particles' stagnation point above the bottom of the furnace is a function of particle diameter: case 3 produces the highest particle stagnation point with the heaviest particles, case 2 produces the lowest with the lightest particles, and case 1's stagnation point falls in between due to the distribution of particle sizes. It is important to note that the overall fuel jet momentum is the same in all cases.

Any differences between cases 1, 2 and 3 are solely due to each particle's momentum.

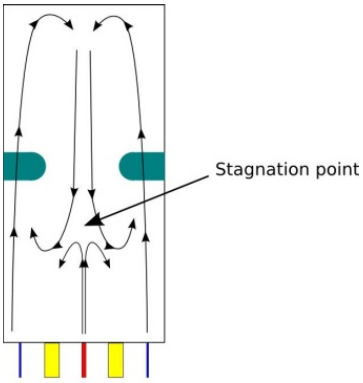

Figure 2: Recirculation pattern observed in the furnace.

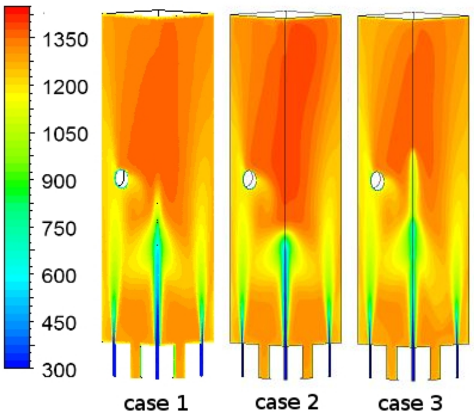

Figure 3: Temperature contours (K) on the symmetry planes for various particle diameters.

In each case, devolatilisation occurs rapidly and is completed before the particles reach the stagnation point. After devolatilisation, MILD combustion proceeds in a manner similar to that of gaseous fuels with little influence from the particles: the high jet momentum of the air creates a strong vortex that entrains the gaseous volatiles which combust in a broad reaction zone, producing a nearly uniform temperature throughout the furnace. The different particle momenta among cases 1-3 yield noticeably different temperature distributions above the fuel jet (Fig. 3). This is because heavier particles have more momentum and thus penetrate deeper into the furnace. Consequently, volatile release and combustion will occur further downstream.

3.2 Effects of Inlet Air Temperatures

Cases 1, 4 and 5 show the effect that increasing inlet air temperature has on furnace operation. Physically, these cases correspond to an increase in jet velocity by air preheating, which adds negligible heat (≤0.5%) to the system and results in similar temperature profiles. In the same way that heavier particles have greater jet penetration, increasing the air jet momentum most noticeably lengthens the air jet cores. Figure 4 shows the mole fraction of O_2 in cases 1, 4 and 5. It is clear that more O_2 reaches the top of the furnace in the higher momentum cases. This has several significant implications on the kinetic rates of reactions (1) and (2). As seen in Fig. 5, increasing the air jet momentum

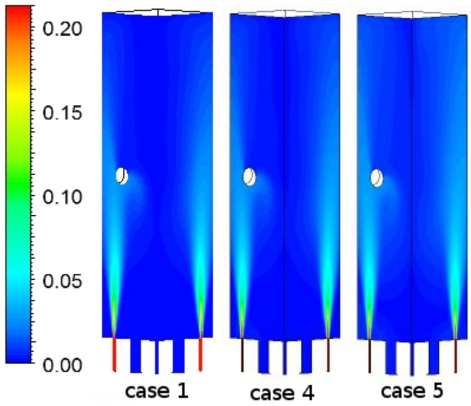

Figure 4: Mass fraction of O_2 contours on the symmetry planes.

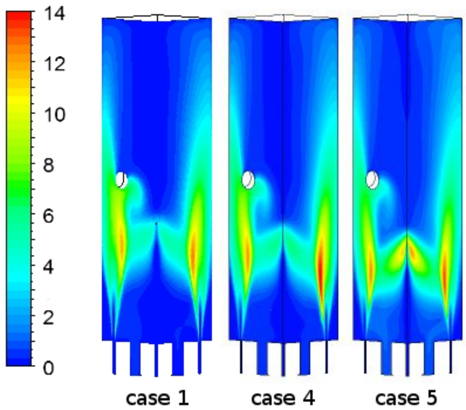

Figure 5: Contours of rates of reaction 1 (mol/m^{3}s) on the symmetry planes.

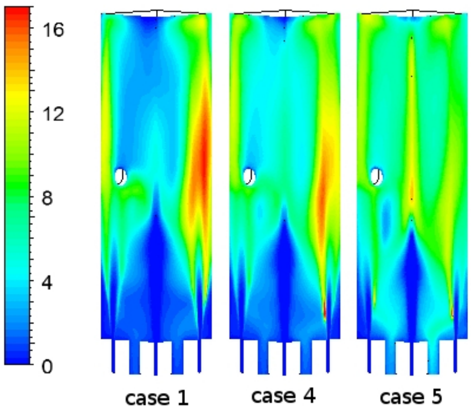

Figure 6: Contours of rates of reaction 2 (mol/m^{3}s) on the symmetry planes.

increases the combustion rate of volatiles (1) in the fuel jet. Because this reaction depends on local O_2 concentration, this increase in reaction rate is due to the increased circulation of air and higher concentration of O_2 near the fuel jet. Figure 6 shows that increasing the air jet momentum diminishes the oxidation rate of CO, but broadens its reaction zone to nearly the entire furnace in case 5. While this does promote MILD combustion, in this furnace it also shifts the reaction zone downward into the exhausts pipes. The result is that more CO escapes the furnace for higher inlet air momentum. For cases 1, 4 and 5, their CO emissions are 1010, 1120, and 1600 ppmv, respectively.

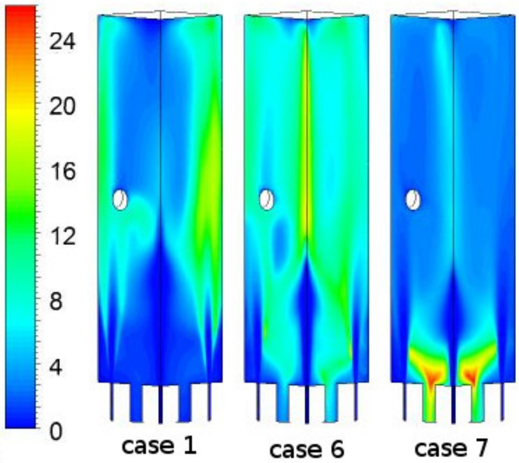

Figure 7: Contours of the kinetic rate of reaction 2 (mol/m^{3}s) on the symmetry planes.

3.3 Effects of Inlet Air Mass Flow Rates

Cases 1, 6 and 7 show an increase in air jet momentum by increasing the air mass flow rate. As with the other cases, longer air jet penetration lengths are observed. In cases 6 and 7, volatiles combust quickly upon release from the coal due to the increased O_2 levels throughout the furnace in the same way as in case 5.

Despite running under leaner conditions, significantly more CO exits the furnace in case 7. For cases 1, 6 and 7, their respective CO emissions are 1010, 1360, and 6910 ppmv. This increase is explained by the reaction zones of reaction 2, shown in Fig. 7. As with case 5, increasing the inlet air momentum in case 6 leads to a broader, more uniform reaction zone and a small increase in CO emissions. In case 7, the air jet momentum is so strong that reaction 2 mostly only happens in or near the exhaust pipe, which accounts for the drastic increase in CO emissions. Although volatile species can combust properly, the momentum of the air jet is too high to entrain and oxidise CO.

4. Conclusions

Simulations of a recuperative MILD combustion furnace were performed to study the effect of increasing the air jet momentum and coal particle momentum on furnace dynamics and global emissions. In all cases, volatiles are released in the fuel jet and carried by a strong vortex induced by the air jets in a manner similar to gaseous MILD combustion. The most significant impact of increasing the air jet momentum, either by raising the temperature or by raising the mass flow rate, is an increased air jet penetration distance. This facilitates volatile combustion and leads to more uniform reaction zones, except in case 7, where the reaction zone is limited to the base of the furnace. This results in insufficient mixing and increased CO emissions, despite leaner operating conditions. The most significant impacts of adjusting the coal particle size are the jet penetration distance and the location of the stagnation point. This modifies the temperature distribution above the fuel jet, but it has little impact on achieving MILD combustion. While the results of these simulations are specific to the Adelaide MILD combustion furnace, they suggest that future experiments must pay special attention to the relative momentum of the air jets, fuel jets, and coal particles to ensure proper mixing, combustion, and circulation. The results may also be helpful in designing new, but similar, recuperative furnaces.

5. Acknowledgements

The authors gratefully acknowledge the Australian-American Fulbright Commission for project funding and eResearch SA for use of their computational facilities. The authors would also like to thank Manabendra Saha for his insights into MILD combustion experiments and Dr Zhao Feng Tian for useful discussions on coal combustion and simulations.

6. References

[1] A. Cavaliere and M. de Joannon, Prog. Energy Combust. Sci. 4 (2004) 329-366.

[2] P. Li, J. Mi, B. Dally, F. Wang, L. Wang, Z. Liu, S Chen, and C. Zheng, Sci. China Tech. Sci. 54 (2011) 255-269.

[3] G. Szegö, B. Dally, and G. Nathan, Combust. Flame. 154 (2008) 281-295.

[4] G. Szegö, B. Dally, and G. Nathan, Combust. Flame. 156 (2009) 429-438.

[5] J. Mi, P. Li, B. Dally, and R. Craig, Energy Fuels. 23 (2009) 5349-5356.

[6] P. Li, B. Dally, J. Mi, and F. Wang, Combust. Flame. 160 (2013) 933-946.

[7] B. Dally, S. Shim, R. Craig, P. Ashman, and G. Szegö, Energy Fuels. 24 (2010) 3462-3470.

[8] H. Stadler, D. Ristic, M. Forster, A. Schuster, R. Kneer, and G. Scheffknecht, 32 (2009) 3131-3138.

[9] M. Vascellari and G. Cau, Fuel, 101 (2012) 90-101.

[10] T. H. Shih, W. W. Liou, A. Shabbir, Z. Yang, and J. Zhu, Computer Fluids. 24 (1995) 227-238.

[11] B. Popoff and M. Braun, International Conference on Multiphase Flow. Leipzig, Germany 2007.

[12] E. H. Chui and G. D. Raithby, Numerical Heat Transfer, Part B. 23 (1993) 269-288.

[13] B. F. Magnussen. "On the Structure of Turbulence and a Generalized Eddy Dissipation Concept for Chemical Reaction in Turbulent Flow", Nineteenth AIAA Meeting, St. Louis 1981.

[14] D. Shaw, X. Zhu, M. Misra, and R. Essehnigh, Proc. Comb. Inst. 23 (1990) 1155-1162.

[15] J. Howard, G. Williams, and D. Fine, Proc. Comb. Inst. 14 (1973) 975-986.

[16] M. Field, Combust. Flame. 13 (1969) 237-252.

[17] D. Smoot and D. Pratt, Pulverised-coal Combustion and Gasification Theory and Applications for Continuous Flow Processes, Plenum Press, 1979.

[18] K. Hsu and A. Jemcov, Numerical Investigation of Detonation in Premixed Hydrogen-air Mixture-assessment of Simplified Chemical Mechanisms, AIAA Paper 2000-2478, Denver, CO, 2000.

[19] H. Kobayashi, J. B. Howard, and A. F. Sarofim, Proc. Combust. Inst. 16 (1977) 411-425.